An Underwater Stable and Durable Gelatin Composite Hydrogel Coating for Biomedical Applications

Luxing Wei [a], Yuan Li [b], Xiaoyong Qiu [c], Xiaolai Zhang [c], Xiaoyu Song [a], Yunpeng Zhao[d], Qing Yu [e], Jinlong Shao [e], Shaohua Ge [e], Jun Huang [a]*

[a] *Center for Advanced Jet Engineering Technologies (CaJET), Key Laboratory of High Efficiency and Clean Mechanical Manufacture of Ministry of Education, School of Mechanical Engineering, Shandong University, Jinan, Shandong, 25006, China*

[b] *Sinopec Research Institute of Petroleum Engineering, Fracturing & Acidizing and Natural Gas Production Research Institute, Dongying, Shandong, 257000, China*

[c] *Key Laboratory of Colloid and Interface Chemistry of the Ministry of Education, School of Chemistry and Chemical Engineering, Shandong University, Jinan 250100, China*

[d] *Department of Orthopaedic Surgery, Qilu Hospital, Cheeloo College of Medicine, Shandong University, Jinan, Shandong, 250012, China*

[e] *Department of Periodontology, School and Hospital of Stomatology, Cheeloo College of Medicine, Shandong University & Shandong Key Laboratory of Oral Tissue Regeneration & Shandong Engineering Laboratory for Dental Materials and Oral Tissue Regeneration & Shandong Provincial Clinical Research Center for Oral Diseases, Jinan, Shandong, 250012, China*

*Email: xyqiu@sdu.edu.cn;

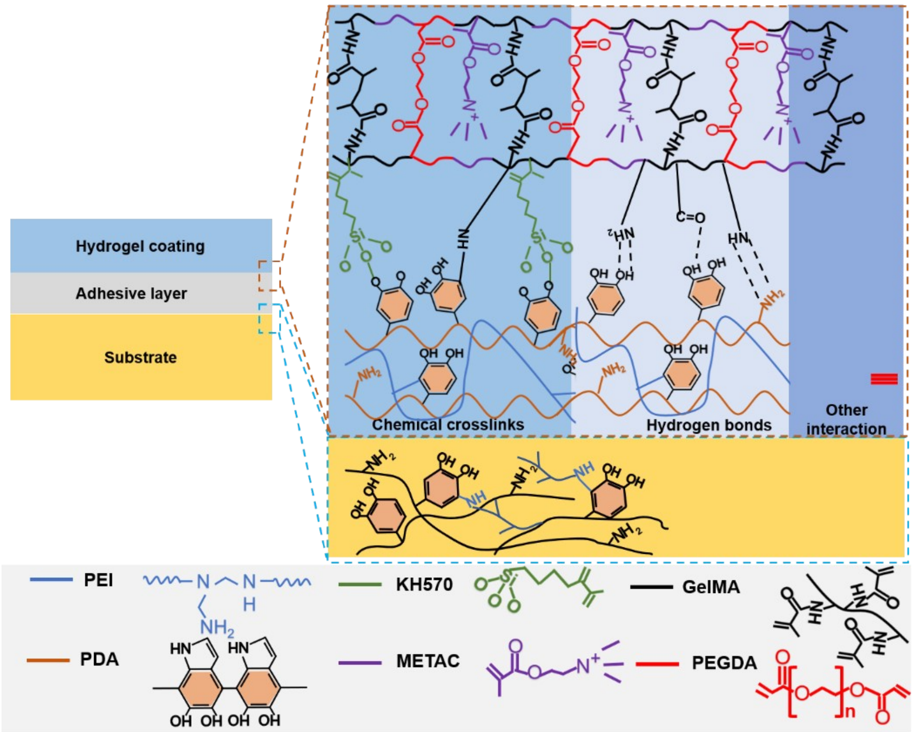

Figure S1 Schematic diagram of the linking interaction between hydrogel coating and substrate.

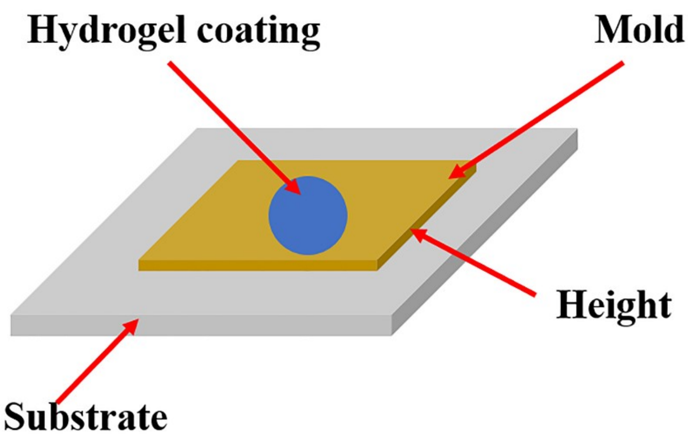

Figure S2 Scheme of tuning the thickness of the hydrogel coating by changing the height of the mold.

Figure S3a shows the surface morphology of the G-M-P-0%, G-M-P-1%, G-M-P-3%, and G-M-P-5% in low magnification (200 ×) and high magnification (1000 ×). After freeze-drying, both the G-M-P-0% and G-M-P-1% exhibit surface undulations at low magnification. Under high magnification, the coating reveals the presence of substantial pores that are notably large and exhibit irregular shapes and sizes. The G-M-

P-3% shows substantial pores under low magnification, and a relatively regular pore structure is found under high magnification. The G-M-P-5% shows a relatively flat surface under low magnification, and tiny undulations and holes can be found under high magnification. The results suggest that an increased content of PEGDA leads to the formation of relatively smooth surfaces, intricate structures, and pores, improving the coating's durability. As shown in **Figure S3b**, the cross-section of the G-M-P-5% is observed. When coated with G-M-P-5%, the surface exhibits a porous structure (**Figure S3a**). The cross-section of the coating shows an obvious layered structure, in which the glass substrate (at the bottom) is compact, and the G-M-P-5% (top layer) is relatively dense.

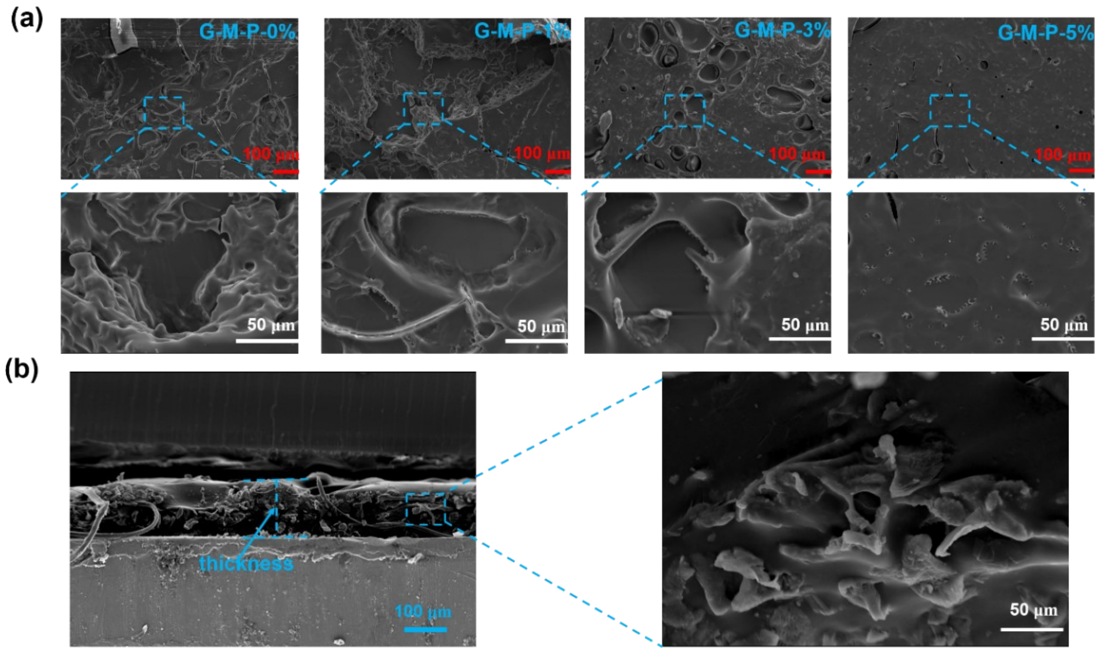

Figure S3 SEM images of GMP coating. **(a)** SEM images of GMP coatings with G-M-P-0%, G-M-P-1%, G-M-P-3%, and G-M-P-5%. **(b)** The cross-sectional morphology of the G-M-P-5%

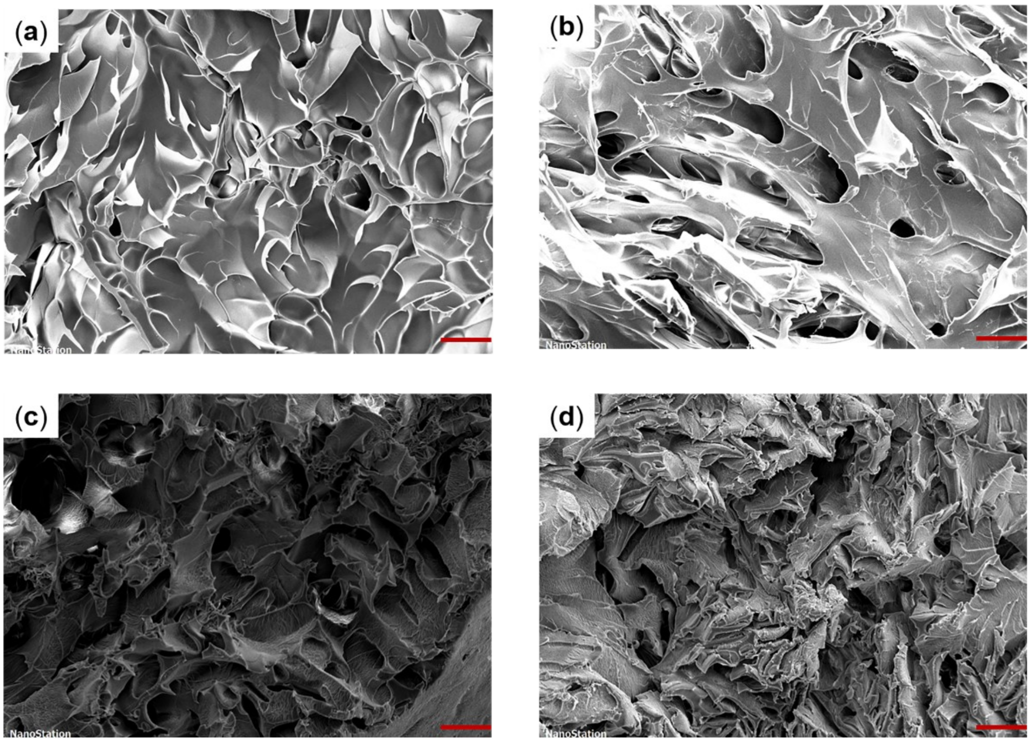

Figure S4 SEM images of hydrogel samples. **(a-d)** SEM images of hydrogel samples with different weight ratios of (GelMA : PEGDA = 10 : 0, 9 : 1, 7 : 3, 5 : 5).

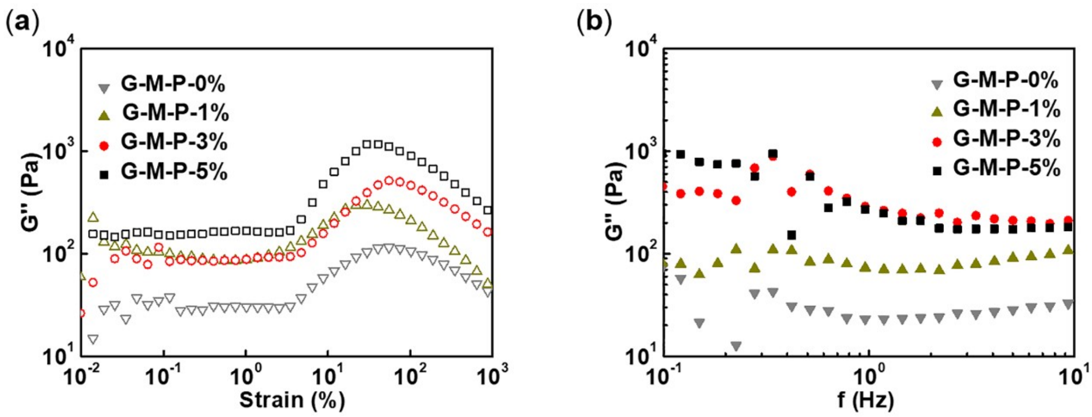

Figure S5 Strain amplitude sweep and frequency tests of hydrogel coating samples. **(a)** Strain amplitude sweep tests of hydrogel coating samples with different weight ratios (GelMA : PEGDA = 10 : 0, 9 : 1, 7 : 3, 5 : 5). **(b)** frequency tests of hydrogel coating samples with different weight ratios (GelMA : PEGDA = 10 : 0, 9 : 1, 7 : 3, 5 : 5).

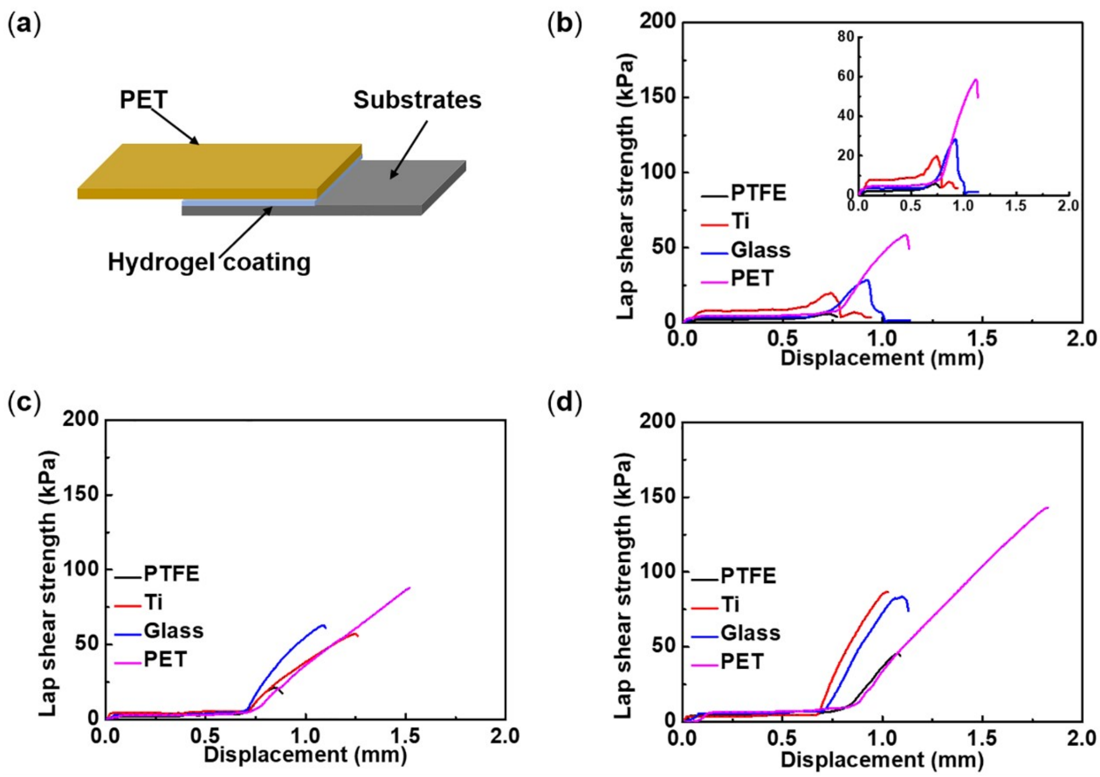

Figure S6 Interface adhesion strength of hydrogel coating. **(a)** The schematic illustration of the lap-shear tests. **(b-d)** The lap-shear adhesion strength curves of the hydrogel coatings on untreated, PDA-PEI-treated, and PDA-PEI-KH570-treated substrates (e.g., PTFE, Ti, Glass, and PET). The adhesion strength tests were repeated three times.

As shown in **Figure S7a and S7b,** the cross-section of the G-M-P-5% is observed before and after underwater ultrasonic treatment. Before underwater ultrasonic treatment, the cross-section of the coating shows an obvious layered structure, in which the glass substrate (at the bottom) is compact, and the G-M-P-5% (top layer) is relatively dense. After underwater ultrasonic treatment, the cross-sectional images reveal the strong adhesion between the coating and the substrate. And due to the swelling of the G-M-P-5% in water, the cross-sectional pores are larger compared to without ultrasound treatment.

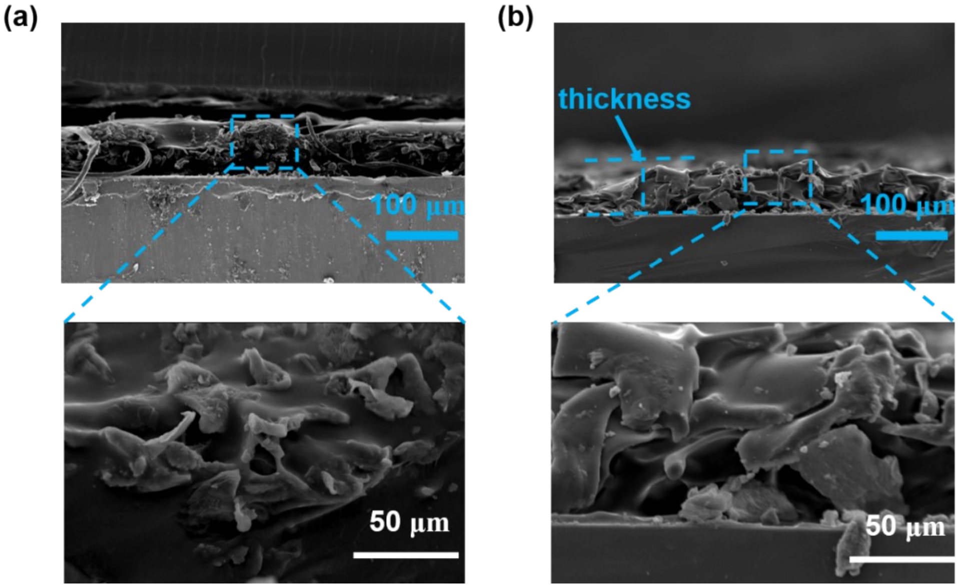

Figure S7 The cross-sectional morphology of the G-M-P-5%. **(a)** Before underwater ultrasonic treatment. the cross-sectional morphology of the G-M-P-5% **(b)** After underwater ultrasonic treatment, the cross-sectional morphology of the G-M-P-5%.

As shown in **Figure S8a and S8b,** the surfaces of the G-M-P-5% appear uniformly smooth after ultrasound treatment, which was accompanied by a slight decrease in water contact angle due to the formation of a hydration layer on the surface.

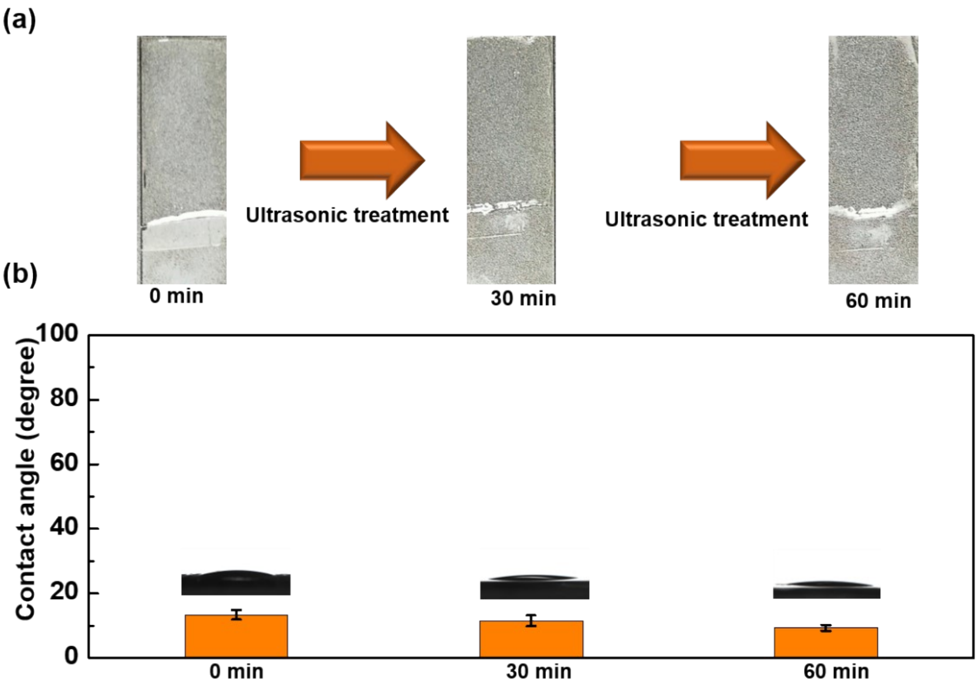

Figure S8 (a) Surface integrity of hydrogel coating before and after underwater ultrasonic treatment. **(b)** The surface wettability tests of the G-M-P-5% before and after underwater ultrasonic treatment.

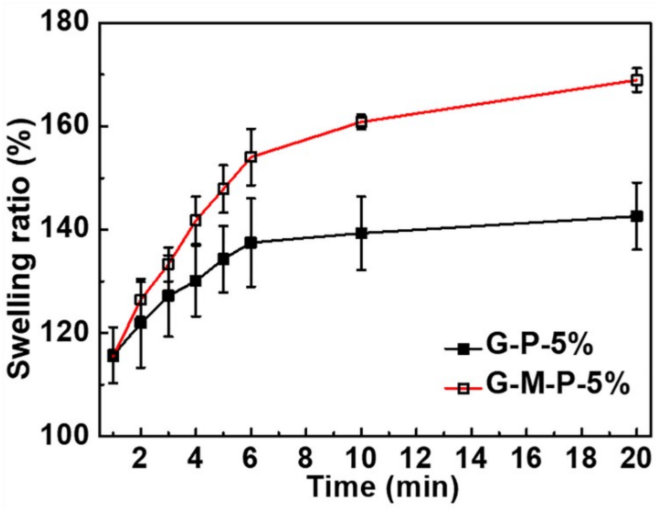

Figure S9 Swelling rate of different hydrogel coatings in PBS (pH = 7.4) at 37 °C with time. The swelling tests were repeated three times.

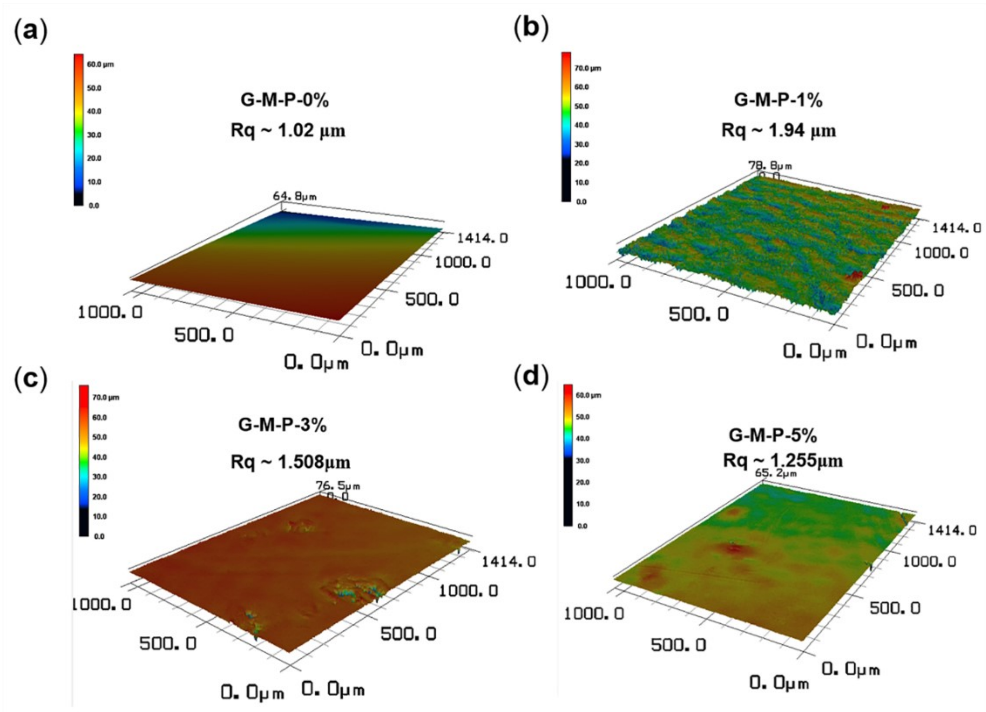

Figure S10 The surface morphology of the hydrogel coating samples before friction tests. **(a-d)** Before friction tests, the R_q roughness values of G-M-P-0 %, G-M-P-1 %, G-M-P-3 %, and G-M-P-5 %, respectively.

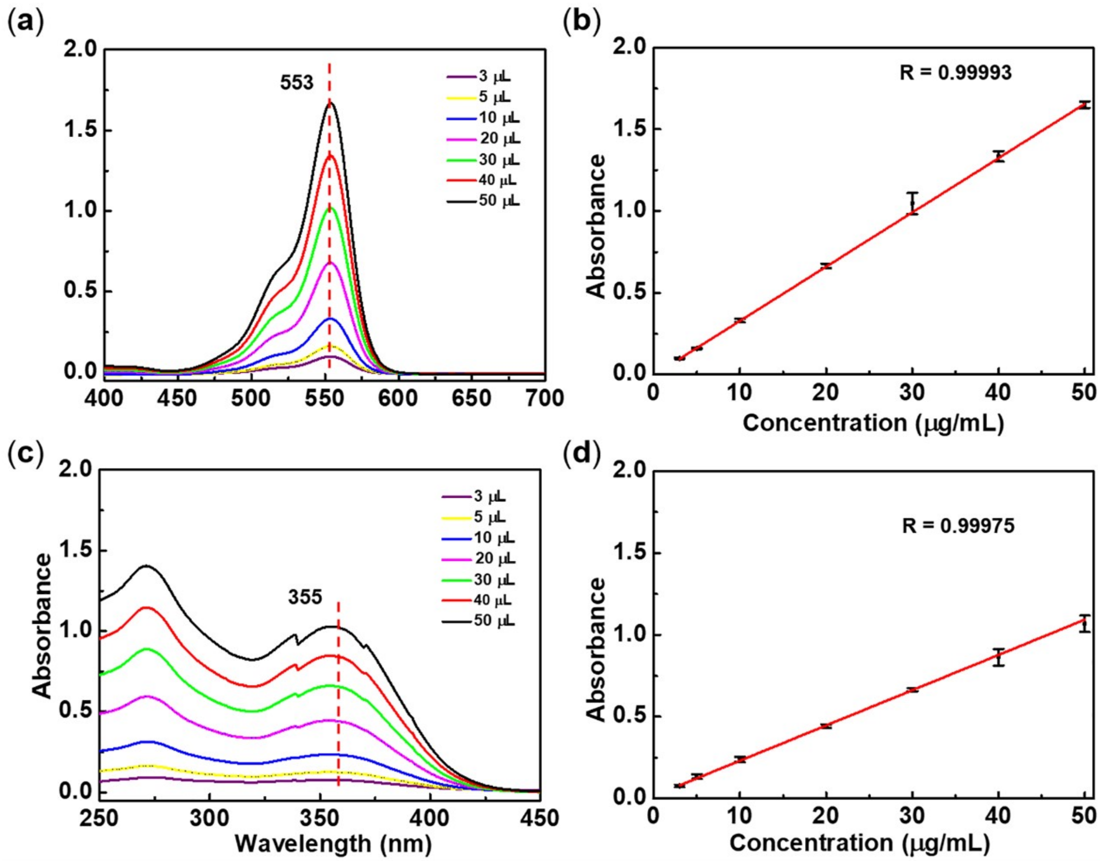

Figure S11 **(a-b)** Standard correlation curve of absorbance and concentration of Rhodamine B in PBS. **(c-d)** Standard correlation curve of absorbance and concentration of doxycycline hydrochloride in PBS.

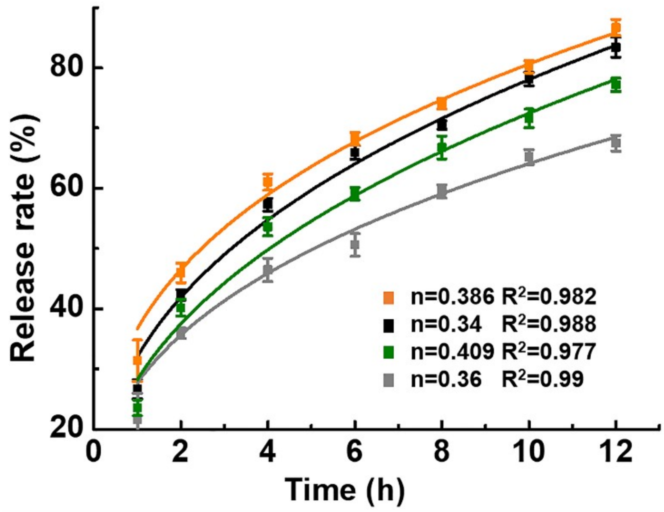

Figure S12 The release curves of doxycycline were fitted by Korsmeyer-Peppas equation.

Table S1. Diffusion exponent and category

diffusion exponent (n)			category
layer	cylinder	sphere	
0.5	0.45	0.43	Fick diffusion
0.5<n<1	0.45<n<0.89	0.43<n<0.85	Anomalous transport
1	0.89	5	Type II transport